New Generation of Zeolite Materials for Environmental Applications.

Ihab Kabalan, Bénédicte Lebeau, Habiba Nouali, Joumana Toufaily, Tayssir Hamieh, Bachar Koubaissy, Jean-Pierre Bellat, Jean Daou

New Generation of Zeolite Materials for Environmental Applications.

Ihab Kabalan[a,b], Benedicte Lebeau[a], Habiba Nouali[a], Joumana Toufaily[b], Tayssir Hamieh[b], Bachar Koubaissy[b], Jean-Pierre Bellat[c], T. Jean Daou[a,*]

a Université de Strasbourg (UDS), Université de Haute Alsace (UHA), CNRS, Equipe Matériaux à Porosité Contrôlée (MPC), Institut de Science des Matériaux de Mulhouse (IS2M), UMR 7361, ENSCMu, 3 bis rue Alfred Werner, F-68093 Mulhouse, France

b Laboratory of Materials, Catalysis, Environment and Analytical Methods, Faculty of Sciences, Doctorate School of Science and Technology, Lebanese University, Lebanon

c Laboratoire Interdisciplinaire Carnot de Bourgogne, UMR 6303 CNRS-Université de Bourgogne Franche-Comté, 9 Av. A. Savary, BP 47870, F-21078 Dijon Cedex, FRANCE

ABSTRACT: The influence of the morphology (microcrystals, nanocrystals, nanosponges and nanosheets) of MFI and *BEA-type zeolites on their adsorption capacities and adsorption rate of n-hexane at 25 °C has been investigated. The capacity of n-hexane adsorption sensitive to micro- and mesopore volume is enhanced by the use of zeolite nanocrystals or hierarchical nanoporous materials (nanosheets and nanosponges). In the case of hierarchical zeolites MFI and *BEA nanosponges, the n-hexane adsorption capacities reached values of about 790 and 693 mg/g, respectively, that are much higher than those in the corresponding microcrystals (130 and 103 mg/g, respectively). On the opposite the kinetics of n-hexane adsorption are slower in nanocrystals and hierarchical zeolites compared to big crystals, due to the lower crystallinity of the zeolitic material and the nature of the probe molecule.

KEYWORDS. Zeolites, Zeolite nanosheets, Zeolite nanosponges, Molecular decontamination, Volatile organic compounds.

INTRODUCTION

The reduction of VOCs emission is an issue of common concern, because these compounds are toxic to the human health and some of them, such as formaldehyde or benzene, are confirmed carcinogens.[1] Moreover, they can lead to severe environmental problems such as the formation of photochemical oxidant species.[2] For this reason, several methods are used to reduce the emission of VOCs such as catalytically-assisted decomposition and trapping in porous material. Nanoporous materials have attracted huge interest among the communities of materials science, chemical engineering, and chemistry due to their excellent properties. Among them, zeolites have attracted increasing interest because of their unique physical and chemical properties, such as high surface area, high chemical resistance, extraordinary mechanical properties, good adsorption and catalytic properties due to specific surface chemistry.[3-5] Zeolites are good candidate for physisorption of small molecules into their micropores. These peculiar properties have highlighted the potential of this material in a variety of applications.[4-10] However, despite their excellent properties, the use of zeolites are limited in many adsorption applications because of their low adsorption capacities and their relatively slow kinetics of adsorption. To overcome this issue, the ideal solutions are to decrease the particle size beyond the nanometer scale and to create additional mesoporosity inside or between zeolite crystals in order to enhance the diffusion and to increase the adsorption capacities of volatile organic compounds.

To improve the mass transfer, the introduction of mesopores into zeolites has recently been achieved using different strategies which gives zeolites with hierarchized porosity.[11-35] Hierarchized porosity can bring many advantages for applications in adsorption, as the increase of the adsorption capacity and the thermal and mechanical stability.[10,36]

MFI and *BEA-type zeolites have been often studied for their high potential for VOC adsorption applications because of their large free microporous volume and their sorption properties. Conventional synthesis of MFI-type zeolites generally lead to the formation of crystals whose size are of the order of several microns and which is characterized by a porous network formed by the interconnection of straight quasi circular channels (5.4 Å x 5.6 Å) with sinusoidal elliptical channels (5.1 Å x 5.4 Å). This structure is of particular interest for several environmental applications such as the removal and/or remediation of anions in water[37] and VOCs in air.[38-44] ZSM-5 and Silicalite-1 are two zeolites with MFI structure that differ on the silicon to aluminum molar ratio of the microporous framework. The latter is a pure silica form whereas zeolite ZSM-5 is an aluminosilicate with Si/Al molar ratios that can vary between 10 and 500. In ZSM-5 the electroneutrality of the framework is counterbalanced by the presence of sodium cations, which constitute specific adsorption sites. *BEA structure type zeolite consists of 3D interconnecting channels formed by 12-membered rings. The pore diameters of the structure are approximately 6.6 × 6.7 Å (linear channels) and 5.6 × 5.6 Å (sinusoidal channels). As ZSM-5, *BEA contains less

or more sodium cations according to its Si/Al ratio. Several sorption tests were led on *BEA-type zeolites, showing excellent affinity for linear alkanes and aromatics such as toluene.[45-48]

In this paper six MFI and *BEA structure-type zeolites exhibiting distinct crystal morphologies were synthesized: microcrystals, nanocrystals, nanosponges and nanosheets. Their structural and textural properties were characterized using XRD, SEM, TEM and nitrogen adsorption techniques. The evolution of their adsorption properties (kinetics and capacities) were then examined by thermogravimetry at 25 °C using n-hexane as probing molecule.

EXPERIMENTAL SECTION

Synthesis of ZSM-5 zeolite (MFI-type structure)

ZSM-5 zeolite large crystals with a coffin shape morphology (denoted as microcrystals) were synthesized in the same condition reported for MFI nanosheets by Dhainaut et al..[49] Sodium hydroxide (Riedel de Haën, 99 %) and $Al_2(SO_4)_3.18H_2O$ (Rectapur, 99 %) were dissolved in deionized water in a 45 ml Teflon-lined stainless steel autoclave. Tetrapropylammonium hydroxide (TPAOH) aqueous solution (20 % in weight, Fluka) and sulfuric acid (Aldrich) were then added under stirring. After homogenization, tetraethoxysilane (TEOS, Aldrich, 98 %) was added dropwise to set the molar composition of the gel to: 100 SiO_2:30 Na_2O:1 Al_2O_3:18 H_2SO_4:20 TPAOH:4000 H_2O. The gel was stirred at 1000 rpm during 4 h at 60 °C prior to be placed in a tumbling oven (30 rpm) at 150 °C for 5 days. The product was recovered by filtration, washed with deionized water and dried overnight at 100 °C. The structuring agent TPAOH was finally removed by calcination in a muffle furnace at 550 °C for 5 h under air.

ZSM-5 zeolites with nanosheet morphology (denoted as nanosheets) were synthesized using $C_{22}H_{45}$-$N^+(CH_3)_2$-C_6H_{12}-$N^+(CH_3)_2$-$C_6H_{13}Br_2$ named (C_{22-6-6}) as organic structure-directing agent as described by Ryoo et al..[7]

A typical ZSM-5 zeolite with a nanosheet morphology (denoted as nanosheets) were synthesized in the same experimental conditions described above for ZSM-5 microcrystals.[7,49] The only difference relied on the use of 0.7 g of C_{22-6-6} as both structure and shape directing agent instead of the appropriate amount of tetrapropylammonium hydroxide (TPAOH). The composition of the gel was therefore 100 SiO_2:30 Na_2O:1 Al_2O_3:18 H_2SO_4:10 C_{22-6-6}:4000 H_2O. After synthesis, the product was recovered by filtration, washed with deionized water and dried overnight at 100 °C. The C_{22-6-6} surfactant was removed by calcination in a muffle furnace at 550 °C for 5 h under air.

ZSM-5 zeolites with nanosponge morphology (denoted nanosponges) were synthesized as described by Na et al.[29] using $C_{18}H_{37}$-$N^+(CH_3)_2$-C_6H_{12}-$N^+(CH_3)_2$-C_6H_{12}-$N^+(CH_3)_2$-$C_{18}H_{37}(Br^-)_3$ named $C_{18-6-6}C_{18}$ as organic structure-directing agent. Sodium hydroxide (Riedel de Haën, 99 %), sodium aluminate (56.7 wt % Al_2O_3, 39.5 wt % Na_2O), tetraethoxysilane (TEOS, Aldrich, 98 %) and ethanol (99 %) were dissolved in deionized water in a 45 ml Teflon-lined stainless steel autoclave. After homogenization, $C_{18-6-6}C_{18}$ was added to set the molar composition of the gel to: 100 SiO_2:22 Na_2O:2.5 Al_2O_3:5 $C_{18-6-6}C_{18}$:800 ETOH:7100 H_2O. The gel was stirred at 1000 rpm for 6 h at 60 °C, and then placed in a tumbling oven (30 rpm) at 140 °C for 4 days. After synthesis, the product was recovered by filtration, washed with deionized water and dried overnight at 120 °C. The $C_{18-6-6}C_{18}$ surfactant was removed by calcination at 550 °C during 4 h in air.

Synthesis of *BEA structure type zeolites

Microcrystals of *BEA-type zeolite (denoted microcrystals) were synthesized following the protocol of Camblor et al.[50] Aluminium powder (Fluka, 99 %) was dissolved in TEAOH solution (Aldrich, 40 % in H_2O) at room temperature under stirring until complete dissolution, and then tetraethoxysilane (TEOS, Aldrich, 98 % in H_2O) was added to the solution and stirred at room temperature in order to evaporate water and obtain a dry gel. Water and HF (Aldrich, 40 % H_2O) were then added to the dry gel for 4 h at room temperature under stirring to obtain a white gel. This gel with the following molar composition 100 SiO_2:6.6 Al:60.6 TEAOH:60.68 HF:706.6 H_2O was kept at 170 °C in a Teflon-lined stainless steel autoclave for 14 days. After filtration the gel was washed with deionized water, dried overnight at 100 °C and calcined at 550 °C for 5 h.

*BEA-type zeolite nanocrystals (denoted nanocrystals) were synthesized using the clear solution method following the protocol of Lauridant et al..[51] TEAOH (Aldrich, 35 % in H_2O), sodium hydroxide (Riedel de Haën, 99 %), and aluminum isopropoxide (Alfa Aesar, 98 %) were dissolved in deionized water at room temperature under stirring until complete dissolution (solution A).

TEAOH (Aldrich, 35 % in H_2O), and ludox AS-40 lyophilized (Aldrich) were dissolved in deionized water at room temperature under stirring until complete dissolution (solution B).

Solution A was added to solution B in a closed polypropylene bottle and the mixture with the following molar gel composition 100 SiO_2:4 Na_2O:20 Al_2O_3:18 TEAOH:1180 H_2O was stirred for 24 h at room temperature. Then the polypropylene bottle was kept at 95 °C for 9 days. The product was recoved by centrifugation at high speed (18000 rpm for 35 min), washed 4 times with deionized water, dried at 100 °C and calcined at 550 °C for 5 h.

beta zeolite with nanosponge morphology (denoted nanosponges) was synthesized as described by Na et al.[29] using $C_{22}H_{45}N^+(CH_3)_2C_6H_{12}N^+(CH_3)_2CH_2pC_6H_4CH_2N^+(CH_3)_2C_6H_{12}N^+(CH_3)_2CH_2PC_6H_4CH_2N^+(CH_3)_2C_6H_{12}N^+(CH_3)_2C_{22}H_{45}(Br)_2(Cl^-)_4$ named N_6-diPhe as organic structure-directing agent.

Sodium hydroxide (Riedel de Haën, 99 %), sodium aluminate (56.7 wt % Al_2O_3, 39.5 wt % Na_2O), tetraethoxysilane (TEOS, Aldrich, 98 %) and ethanol (99 %) were dissolved in deionized water in a 45 ml Teflon-lined stainless steel autoclave. After homogenization, N_6-diPhe was added to set the molar composition of the gel to: 100 SiO_2:22 Na_2O:2.5 Al_2O_3:5 N_6-diPhe:800 ETOH:7100 H_2O. The gel was stirred at 1000 rpm during 6 h at 60 °C, and then placed in a tumbling oven (30 rpm) at 140 °C for 4 days. After synthesis, the product was recovered by filtration, washed with deionized water and dried overnight at 120 °C. The N_6-diPhe surfactant was finally removed by calcination at 550 °C during 4 h in air.

Characterizations

X-ray diffraction patterns of the different materials were recorded using a PANalytical MPD X'Pert Pro diffractometer operating with Cu Kα radiation (λ= 0.15418 nm) equipped with an X'Celerator real-time multiple strip detector (active length = 2.122° 2θ).

The morphology, homogeneity and particle sizes of the synthesized materials were investigated with a scanning electron microscope (SEM) (Philips XL30 FEG) and a transmission electron microscopy (TEM) using a Philips model CM200, under an acceleration voltage of 200 kV, with a point-to-point resolution of 0.3 nm. Nitrogen adsorption–desorption isotherms were obtained at -196 °C by using a Micromeritics ASAP 2420 apparatus. The samples were out-gassed under vacuum for 1 h at 90 °C then at 300 °C overnight before the measurements. Surface area was calculated according to the BET method using the following areas $2.10^{-4} < p/p_o \leq 8.10^{-2}$ and $4.10^{-3} < p/p_o \leq 12.10^{-2}$ for microcrystals and hierarchical materials (nanosheets, nanosponges, nanocrystals) respectively.[52,53] The microporous volumes (V_{micro}) were calculated using the t-plot method. The pore size distribution was determined by using the Barrett–Joyner–Halenda (BJH) model applied on the desorption branch and the Density Functional Theorie (DFT) model applied on the adsorption branch.[52,53] The total pore volume was calculated at $p/p_o = 0.9$.

N-hexane adsorption measurements

N-hexane adsorption-desorption isotherms

N-hexane adsorption and desorption isotherms were obtained at 25 °C from thermogravimetric measurements by using a McBain balance.[54] About 15 mg of the sample previously activated at 300 °C for 12 h at 10^{-2} Pa pressure were exposed to pure hexane vapor under well-controlled -cold point- conditions. The adsorption-desorption isotherm is obtained by performing successive increments and decrements of pressure once an equilibrium of mass is reached, respectively.

Dynamic n-hexane adsorption measurements

Dynamic adsorption measurements were performed under VOC atmosphere (n-hexane) at 25 °C and controlled value of relative pressure $p/p_o = 0.5$ (p is the vapor pressure and p0 is the saturation vapor pressure of n-hexane at 25 °C (p_o = 202 hPa) using a thermogravimetric Setaram TG92 instrument.[34,44] The experiments were done under N_2 flow.

The relative pressure $p/p_o = 0.5$ was obtained by setting the pressures of auxiliary gas (N_2 + n-hexane) and carrier gas (N_2) to 1.5 bar at the inlet of the oven and controlled by measuring the gas flow rate at the outlet of the oven. The gas flow rate was stable (114 ml/min). The experiment begun with an activation phase: the zeolithes were heated up to 350 °C under dried nitrogen for 2 h at atmospheric pressure to remove all adsorbate traces. Then, the sample was cooled to 25 °C, and the organic compound was introduced to the system. The adsorbed amount was then measured every 20 s.

RESULTS AND DISCUSSION

Characterization of the zeolites

The crystallinity and purity of the zeolite samples were checked by XRD. Figures 1 and 2 show the X-ray diffractograms of ZSM-5 and beta zeolites with different morphologies: microcrystals, nanocrystals, nanosheets and nanosponges. According to the XRD patterns reported in figure 1b, the conventional ZSM-5 sample synthesized in the presence of TPA^+ cation is a pure and well crystallized MFI-type zeolite. The use of $C_{22\text{-}6\text{-}6}$ as structure directing agent, generates nanosheets with mesostructuration identified by the presence of broad peaks at low diffraction angles as shown in figure 1a (1.6 ° < 2θ < 4.2 °). These peaks disappear after calcination, indicating that the organization of materials at the mesoscopic scale is due to the presence of $C_{22\text{-}6\text{-}6}$ which acts as structure and shape directing agent. At the wide angles, only the diffraction peaks relative to crystallographic planes (hol) are strong enough to be properly indexed in the orthorhombic system of MFI, thus indicating the growth inhibition along the b-axis. As-made nanosponges obtained after changing the template nature ($C_{18\text{-}6\text{-}6}C_{18}$ instead of $C_{22\text{-}6\text{-}6}$) and optimizing the synthesis conditions show also a mesostructure characterized by a broad peak at low angle corresponding to 2θ = 1.3° (Figure 1a).

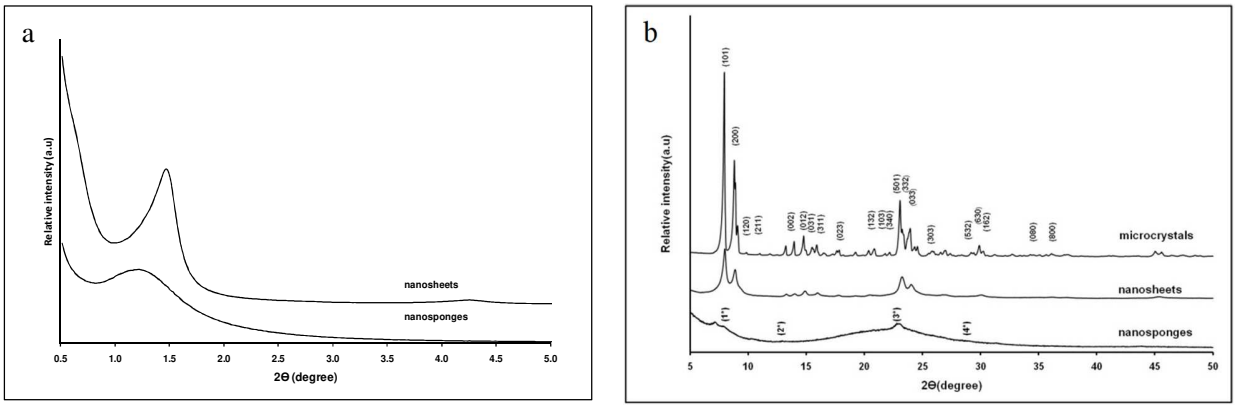

Figure 1. a) Low angle XRD patterns of as-made ZSM-5 nanosheets and nanosponges and b) wide angle XRD patterns of the calcined microcrystals, nanosheets and nanosponges ZSM-5 zeolites.

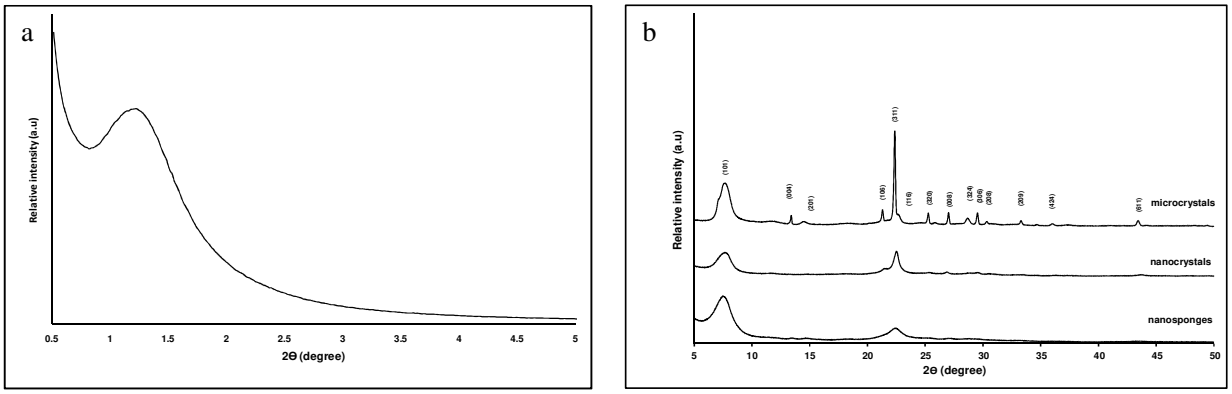

Figure 2. a) Low angle XRD pattern of the calcined beta nanosponges and b) wide angle XRD patterns of the calcined microcrystals, nanocrystals and nanosponges *BEA-type zeolites.

Unlike nanosheets this broad peak remains intact after calcination suggesting a higher mesoporous volume for nanosponge sample as it will be shown below. According to Na et al. [29] all reflections observed in the wide angle XRD region for calcined nanosponge MFI-like zeolite suggest a 2D hexagonal symmetry, similar to MCM-41. The XRD resolution is not sufficient to distinguish correctly the reflection peaks, which may be explained by the small crystallite sizes as it will be shown below by SEM and TEM images (Figure 3c, 4b).

The *BEA phase was clearly observed for all beta zeolite samples (figure 2b). The XRD reflections of beta nanocrystals and beta nanosponges are less intense and broader than those of the beta microcrystals. A broad peak was observed at low angles for as-made beta nanosponges indicating a mesotructration due to the presence of the organic agent.

The SEM and TEM images displayed in figures 3 and 4, respectively, show the different morphologies observed for the ZSM-5 and beta synthesized zeolites. Micrometric crystals with parallelepiped shape were obtained for the ZSM-5 microcrystals (figure 3a), with an average size of of 5-7 μm. The replacement of TPAOH by the bifunctional organic compound $C_{22\text{-}6\text{-}6}$ generates the production of lamellar materials that are called nanosheets (figure 3b, 4a). The overall thickness of the lamellar stacking of nanosheets was about 20-40 nm as shown in figure 4a. The thickness of each nanosheet was 2 nm. The increase of the carbon length chain and the number of quaternary ammonium of the used structuring agent ($C_{18\text{-}6\text{-}6\text{-}18}$) lead to nanosponge morphology (Figure 3c, 4b). The morphology of nanosponges was spiky nanomaterials that are uniform in size and shape as shown from SEM image.[13,29]

In the case of beta microcystals, truncated bipyramidal crystals with an average size of 6-10 μm are observed (figure 3d). The synthesis realized by applying the clear solution method in the presence of TEAOH has lead to the formation of beta nanocrystals with pseudo spherical morphology and an average size of 40 nm (figure 3e, 4c).

In contrast, *BEA-type zeolites synthesized in the presence of N_6-diphe surfactant exhibit a nanosponge morphology (figure 3f, 4d). According to the TEM (figure 4d), the nanosponges are constituted by randomly aggregated nanoparticles delimited by mesoporous channels. Moreover, the presence of nano-sized beta crystals with a size close to 4

nm separated by channels of approximately 4 nm in diameter were observed.

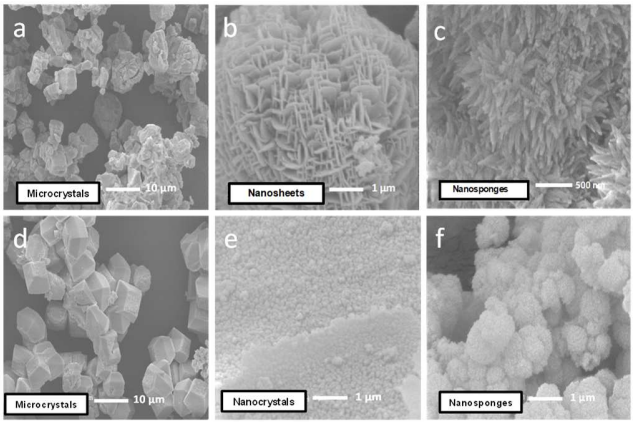

Figure 3. Scanning electronic microscopy (SEM) images of MFI (a,b,c) and *BEA (e,f,g) type zeolites with different morphologies.

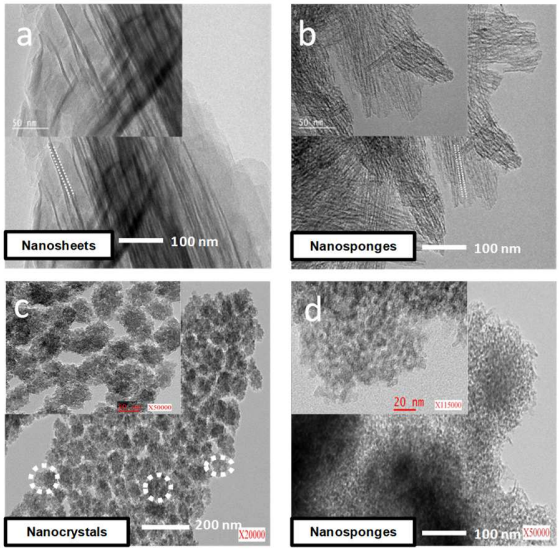

Figure 4. Transmission electronic microscopy (TEM) images of MFI (a,b) and *BEA (c,d) type zeolites with different morphologies.

The textural properties of the ZSM-5 and beta zeolites with different morphologies were investigated by adsorption-desorption of nitrogen. Figure 5 shows the N_2 adsorption-desorption isotherms of the calcined ZSM-5 samples. The isotherm of microcrystals is of type I, with a micropore volume of 0.19 cm^3/g. The adsorption isotherm of nanosheets is of type I at low p/p_o, and of type II with H4 hysteresis at high p/p_o.[52,53] The presence of an hysteresis loop in the relative pressure range $0.4 < p/p_o < 1$ is typical of lamellar materials, due to the stacking of nanosheets. The nanosponges have a type Ib isotherm at low p/p_o with a micropore volume (0.3 cm^3/g) higher than those obtained for the other two morphologies (see table 1). This can be explained by the presence of secondary micropores in the structure of the material. The secondary micropores are additional micropores (in addition to the channels due to MFI-type zeolite framework) induced by the presence of $C_{18\text{-}6\text{-}6}C_{18}$ in the synthesis gel. At high p/p_o the isotherm is similar to type IV and II (with H4 hysteresis) indicating the presence of mesopores (capillary condensation step around $p/p_o = 0.6$) and textural porosity (interparticle adsorption at $p/p_o > 0.9$), respectively. The BJH pore size distribution of nanosponge sample is monomodal, quite narrow with a mean pore diameter of about 3.7 nm. For nanosheet sample, the BJH pore size distribution is much less intense and broader with a maximum at 3.6 nm. For this case, the DFT method does not allow to determine an averagepore size whereas for nanosponge sample an average pore size arround 4.6 nm could be measured. The Brunauer- Emmett- Teller (BET) surface area, microporous and mesoporous volumes are reported in table 1. The total pore volume and BET surface increase from microcrystals to nanosheets and from nanosheets to nanosponges.

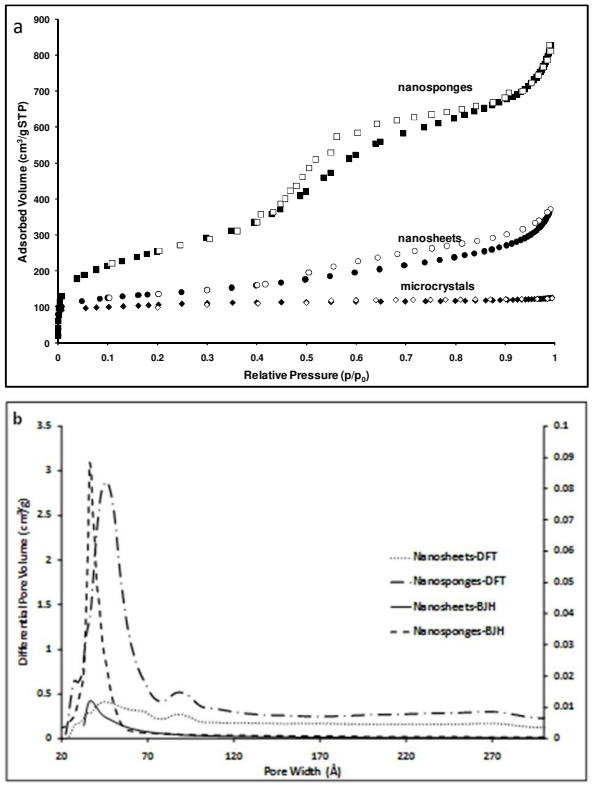

Figure 5. a) Adsorption-desorption isotherms of nitrogen on the calcined MFI-type zeolites (microcrystals, nanosheets and nanosponges) at -196 °C [closed symbols:

adsorption; open symbols: desorption]. b) BJH and DFT pore size distributions determined from the desorption branch and adsorption branch, respectively.

Figure 6 displays the N_2 adsorption-desorption isotherms of the calcined *BEA zeolites with different morphologies. As expected for microporous solids adsorption-desorption isotherms are of type I in the low p/p_0 range. The nanocrystals present an isotherm of the type Ib and IV. The step at high p/p_0 relative pressures (0.75-0.95) indicates the presence of external interparticle mesoporosity which is due to the agglomeration of the zeolite nanoparticles. According to the BJH and DFT methods the pore size distribution of the nanocrystal sample is between 12 and 42 nm and 10 and 72 nm respectively. The isotherm of nanosponges is of type Ib and IV (figure 6). The mesopores revealed by the step in the p/p_0 = 0.5-0.95 range are generated by the use of the N_6-diphe structure and shape directing agent and are characterized by a high adsorbed volume (mesoporous volume). The BJH pore size distributions of nanosponges is monomodal and quite narrow with an average pore diameter of 4.8 nm for nanosponges. The DFT pore size distribution for nanosponge samples give an average pore diameter of 5 nm similar to the one obtained by the BJH method. The associated Brunauer-Emmett-Teller (BET) surface area, microporous and mesoporous volume of the three morphology of *BEA-type zeolites are reported in table 1. The presence of mesopores in hierarchized zeolites results in higher total pore volumes, 1 cm^3/g for nanocrystals and nanosponges, with specific surface areas of 833 and 807 m^2/g respectively. For both nanocrystals and nanosponges the type Ib indicates the presence of supermicropores that are due to defaults generating thus additional micropore volume.

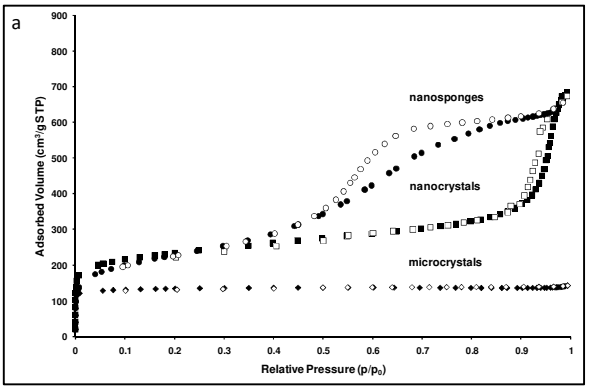

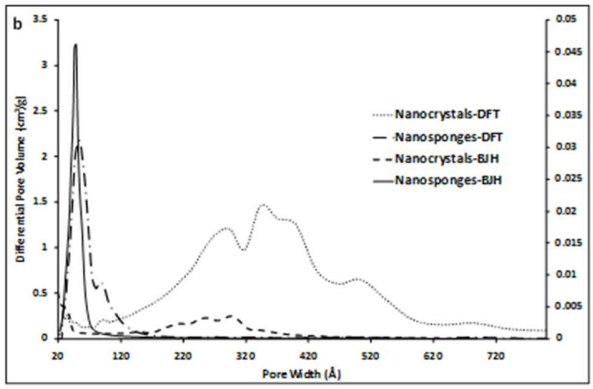

Figure 6. a) Adsorption-desorption isotherms of nitrogen on the synthesized *BEA-type zeolites (microcrystals, nanocrystals and nanosponges) at -196 °C [closed symbols: adsorption; open symbols desorption]. b) BJH and DFT pore size distributions determined from the desorption branch and adsorption branch, respectively.

Table 1. Textural properties of the calcined MFI and *BEA-type zeolites.

Zeolite structure type		S_{BET} ($m^2.g^{-1}$)	V_{tot} ($cm^3.g^{-1}$)	V_{micro} ($cm^3.g^{-1}$)	V_{meso} ($cm^3.g^{-1}$)
MFI	Microcrystals	394	0.19	0.19	-
	Nanosheets	492	0.54	0.18	0.36
	Nanosponges	888	1.28	0.30	0.98
*BEA	Microcrystals	524	0.22	0.22	-
	Nanocrystals	833	1	0.27	0.73
	Nanosponges	807	1	0.30	0.70

Adsorption-desorption isotherms of n-hexane

Adsorption-desorption isotherms of n-hexane in ZSM-5 zeolites

The adsorption-desorption isotherms of n-hexane in MFI-type zeolites are shown in figure 7. The microcrystals exhibit an isotherm of type I, characteristic of microporous solids. Sorption isotherms at 25 °C are reversible and do not show any hysteresis upon desorption. At low-pressure a sharp slope of the adsorption isotherm is observed indicating a strong adsorption affinity of the MFI zeolite for n-hexane. Moreover, the plateau of the isotherm is reached at

a low value of pressure, which corresponds to p/p_o = 0.1. We note that the maximum adsorption capacity reaches 130 mg/g (0.198 cm^3/g) which corresponds to 8.68 n-hexane molecules per unit cell. This result is in good agreement with data reported in the literature (see table 2) and with the adsorbed volume of nitrogen observed above (0.19 cm^3/g) which means that all the porosity is occupied by n-hexane.[38,44,55-58]

In the case of hierarchical zeolites, the isotherms are of type I and II for nanosheets and of type IV for nanosponges (figure 7). The total n-hexane adsorbed amounts increases with the increasing of the pore volumes due to the presence of mesoporosity. Concerning the nanosheets, the n-hexane adsorption capacity reached 180 mg/g at pressure p/p_o = 0.1 and increased with increasing relative pressure to reach 290 mg/g (0.442 cm^3/g) at p/p_o = 0.9 as a consequence of the filling of the mesopores. However, the adsorption-desorption isotherm of n-hexane on nanosponges, show that the adsorption in micropores is low and occurs preferentially in mesopores to reach a value of 790 mg/g (1.205 cm^3/g) at p/p_o = 0.9. Taking into account these results, the adsorbed amount of n-hexane was multiplied by 2.2 and 6 in the case of ZSM-5 nanosheets and nanosponges respectively compared to conventional microcrystals.

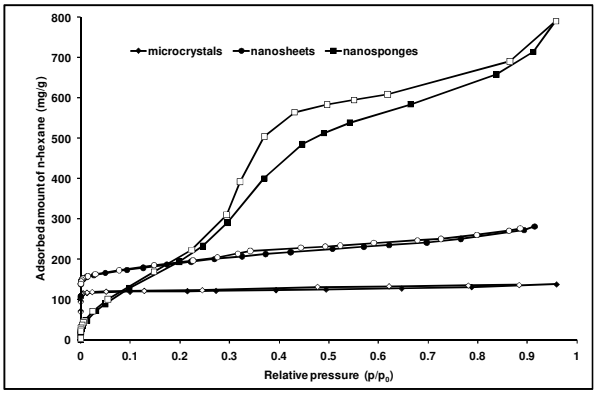

Figure 7. Adsorption-desorption isotherms of n-hexane on MFI-type zeolites (microcrystals, nanosheets and nanosponges) at 25 °C [closed symbols: adsorption; open symbols: desorption).

Adsorption- desorption isotherms of n-hexane in beta zeolites

The adsorption-desorption isotherms of n-hexane in *BEA-type zeolites are shown in figure 8.

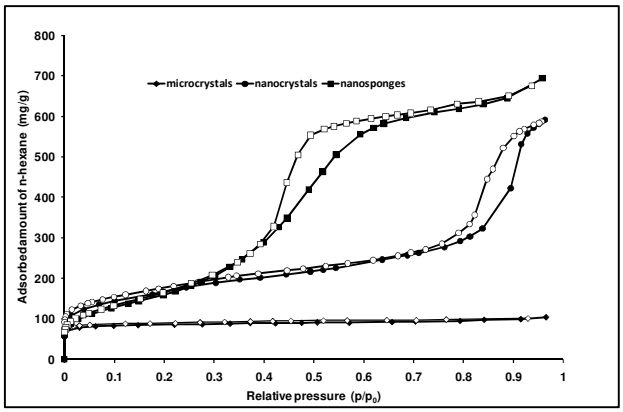

Figure 8. Adsorption-desorption isotherms of n-hexane on *BEA-type zeolites (microcrystals, nanocrystals and nanosponges) at 25 °C [closed symbols: adsorption; open symbols: desorption).

The shapes are similar to those of N_2 adsorption-desorption. Microcrystals shows an isotherm type I which characterize the microporous materials. The formation of a plateau indicating the saturation of micropores is noticed in the p/p_o range from 0.1 to 1. At p/p_o = 0.1 all micropores are filled with an adsorbed amount of 103 mg/g (0.157 cm^3/g) corresponding to 4.6 molecules per unit cell.[38,44,55-58] Comparable profiles of the adsorption of n-hexane on the nanocrystals and nanosponges were observed at low pressure at p/p_o = 0.1 with adsorption values around 140 and 130 mg/g respectively. At p/p_o value of 0.9, the adsorption capacities in nanocrystals and nanosponges reached 591 and 693 mg/g (0.901 and 1.057 cm^3/g), respectively. These values are in good agreement with the adsorbed volume of nitrogen observed above (1 cm^3/g for both samples) which means that all the porosity is occupied by n-hexane. Taking into account these results, the adsorbed amount of n-hexane was multiplied by 5.7 and 6.7 in the case of beta nanocrystals and nanosponges respectively compared to conventional microcrystals.

MFI and *BEA nanosponges are promising materials because they possess higher adsorption capacities and affinities of n-hexane compared to the most used mesoporous materials (SBA-15 and MCM-41) and activated carbon. These hierarchical zeolite materials possess the advantage to begin the adsorption of the VOCs present at low pressures due to the presence of micropores which is not the case of mesoporous materials where the the VOCs have to be at high partial pressure in order to fill the pores. This is not the situation with most industrial applications where some VOCs are normally present at low pressures.

Table 2. Adsorption capacity of n-hexane in MFI and *BEA-type zeolites from the literature compared to the results of this study.

Zeolite structure type	Temperature (°C)	Adsorbed amount (mg/g)	Adsorbed volume[a] (cm^3/g)	Reference
MFI	20	122.36	0.185	Wu et al.[38]
MFI	25	116	0.176	Long et al.[55]
MFI	22	115	0.174	Kirsch[56]
MFI	25	110.3	0.168	Cosseron et al.[44]
MFI	90	80	0.135	Xu et al.[57]
MFI	25	138.7	0.211	Ferreira et al.[58]
MFI	25	130	0.198	Our work
MFI	25	290	0.442	Our work
MFI	25	790	1.205	Our work
*BEA	25	186.5	0.284	Reddy et al.[46]
*BEA	22	134	0.202	Kirsch[56]
*BEA	25	108	0.164	Cosseron et al.[44]
*BEA	200	53.1	0.123	Bárcia et al.[59]
*BEA	25	103	0.157	Our work
*BEA	25	591	0.901	Our work
*BEA	25	693	1.057	Our work
SBA-15	25	653	0.990	Van Bavel et al.[60]
MCM-41	22	600	0.901	Zhao et al.[61]
Activated carbon	22	325	0.493	Zhao et al.[61]

[a] the adsorbed volume of n-hexane was determined using the following formula : adsorbed amount of n-hexane (mg/g).$10^{-3}/\rho(cm^3/g)$; where ρ is the density of liquid n-hexane at the working temperature.

N-hexane adsorption kinetics

N-hexane adsorption kinetics in ZSM-5 zeolites

Adsorption kinetics of n-hexane in the different morphology of MFI-type zeolites at 25 °C and p/p_0 = 0.5 are presented in figure 9.

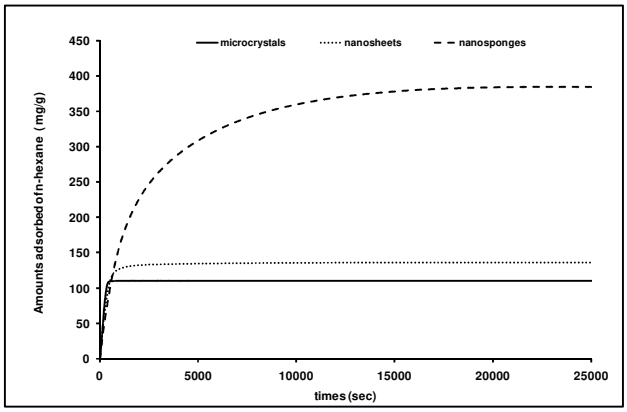

Figure 9. Adsorption kinetics of n-hexane in MFI-type zeolites having different morphologies (at 25 °C and p/p_0= 0.5).

The quantification of the diffusion properties in the ZSM-5 zeolites was achieved using Fick's second law (equation 1), which describes the change of the molecule concentration inside the zeolite crystals as a function of time.[62]

In the case of 3-dimensional space, the diffusion equation is:

$$\frac{\partial n(M,t)}{\partial t} = D\Delta n(M,t) \quad (1)$$

Where Δn (M, t) represents the Laplacian of n (M, t).

The solvation of the second Fick law for an adsorbent particle of any arbitrary shape placed in a gas phase of constant concentration leads, for short times, to the relation[62,63]:

$$\frac{q(t)}{q(m)} = \frac{2}{\sqrt{\pi}}\sqrt{\frac{D}{r^2}}\sqrt{t} \quad (2)$$

q(t) is the amount adsorbed at the time t and q(m) is the maximal amount adsorbed at equilibrium i.e when time tends to infinity. The ratio q(t)/q(m) is the extent coefficient of the reaction so-called the normalized loading. D is the diffusion coefficient. r is called the diffusion length and is defined by the ratio of particle volume to external surface area r = V/S. Thus the diffusion coefficient can be determined from the slope of the plot normalized loading versus square root of time for the initial stage of uptake.

For all the samples the plot of the normalized loading as a function of the square root of time leads almost to a straight line, as shown in figure 10.

Although the model does not fit very well the experimental data, the fitted data were used to analyze the tendencies. From straight lines the characteristic diffusion times (r^2/D) of 404 s for the microcrystals, 715 s for the nanosheets and 4567 s for the nanosponges were determined. The diffusion time indicates a much slower diffusion in nanosponges

than in nanosheets and microcrystals ($r^2/D_{nanosponges} <<< r^2/D_{nanosheets} < r^2/D_{microcristals}$). This increase of the diffusion time can be attributed according to Xu et al.[57] to the low cristallinity and edge effect, where only part of the molecule is confined in micropore opening or to the nature of the crystal surface which can highly influence the diffusion time of VOCs through zeolites, as mentioned by Gueudré *et al.*[64] This phenomenon is more pronounced for low diffusion time which is our case here, when using *n*-hexane as probe molecule.This is consistent with our structural characterization which showed a decrease in the crystallinity of materials when creating the mesopores.

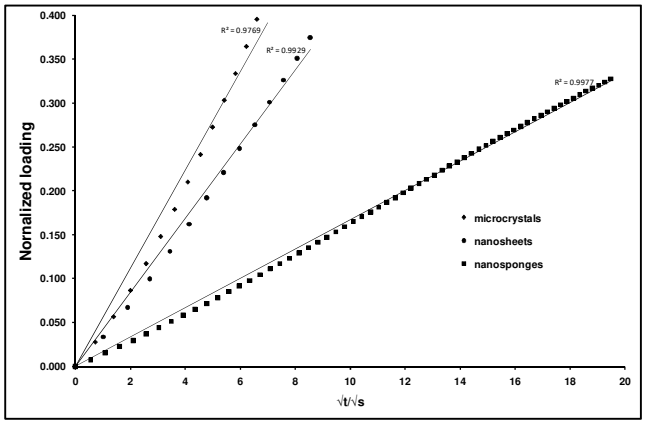

Figure 10. Normalized uptake in short time of MFI-type zeolites having different morphologies (at 25 °C and p/p_o= 0.5). Straight lines correspond to fitted data by equation (2).

Adsorption kinetics in beta zeolite

The kinetics curves of n-hexane adsorption in beta zeolites are presented in figure 11.

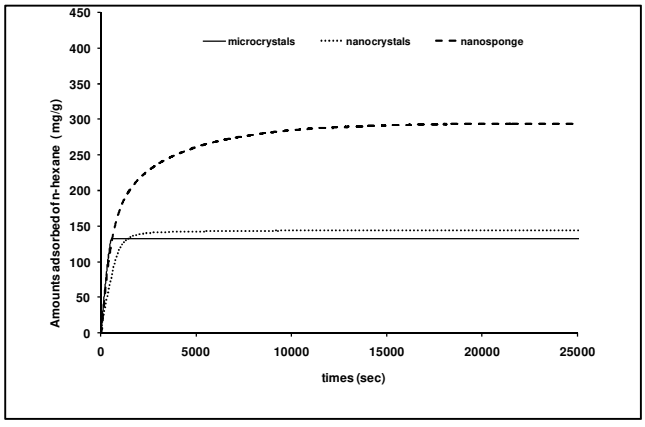

Figure 11. Adsorption kinetics of n-hexane in *BEA-type zeolites having different morphologies (at 25 °C and p/p_o= 0.5).

The diffusion coefficients in the three morphologies are established using the Fick law as shown in figure 12. The correlation coefficients between experimental and fitted data are low but tendencies can be deduced from the used model. From straight lines the characteristic diffusion times (r^2/D) of 812 s for the microcrystals, 2139 s for the nanocrystals and 1834 s for the nanosponges were determined. We can note that the diffusion time is faster in microcrystals than in nanocrystals and nanosponges. The increase in the diffusion time is related to the lower crystallinity and to the arrangement of the mesopores inside the synthesized samples. We have shown above in the structural characterization part that the crystallization decreases while decreasing the particle size and that the nanosponge material presents an organized mesoporosity at the long range which is not the case of beta nanocrystals. An influence of the nature of the external crystal surface as mentioned by Gueudré et al.[64] is not to excludes. Beta nanocrystals and nanosponges are micro- and mesoporous with a large fraction of mesopores that slow down the diffusion of probe molecule, while microcrystals presented only micropores.

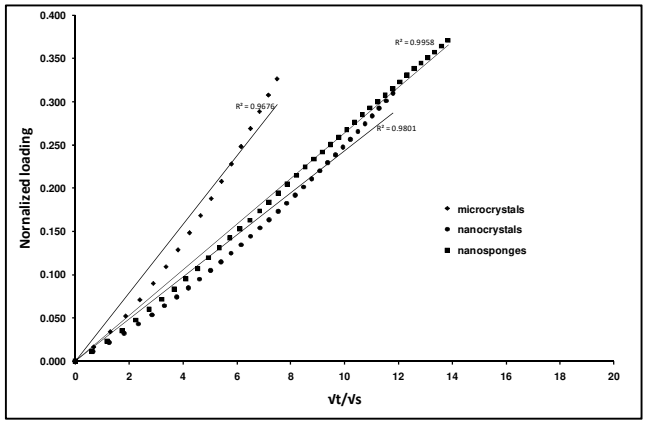

Figure 12. Normalized uptake in short time of *BEA-type zeolites having different morphologies (at 25 °C and p/p_o= 0.5). Straight lines correspond to fitted data by equation (2).

Table 3. Diffusion times of n-hexane in MFI and *BEA-type zeolites at 25 °C and p/p_o = 0,5.

Zeolite structure-type and morphology		**Diffusion times r^2/D (s)**
MFI	Microcrystals	404
	Nanosheets	715
	Nanosponges	4567
***BEA**	Microcrystals	812
	Nanocrystals	2139
	Nanosponges	1834

CONCLUSIONS

Six MFI and *BEA structure-type zeolites exhibiting distinct crystal morphologies were synthesized and fully characterized: microcrystals, nanocrystals, nanosponges and nanosheets. The evolution of their adsorption properties (kinetics and capacities) were then examined by thermogravimetry at 25 °C using n-hexane as probing molecule.

MFI and *BEA microcrystals are microporous materials and exhibit the lowest adsorption capacity for n-hexane due to their lower pore volume but the highest diffusion time compared to hierarchical zeolites (nanocrystals, nanosheets, nanosponges). The adsorbed amount of n-hexane was multiplied by 2.2 and 6 in the case of ZSM-5 nanosheets and nanosponges respectively compared to conventional ZSM-5 microcrystals and by 5.7 and 6.7 in the case of beta nanocrystals and nanosponges respectively compared to conventional microcrystals. The increase of diffusion time in hierarchical zeolites can be explained by the lower crystallinity of the hierarchized material and the nature of external crystal surface.

These hierarchical zeolites are promising adsorbents for technological use in molecular decontamination.

Corresponding Author

* Corresponding author: jean.daou@uha.fr, Telephone number: +33 3 89 33 67 39, Fax number: +33 3 89 33 68 85

Author Contributions

The manuscript was written through contributions of all authors. / All authors have given approval to the final version of the manuscript. / ‡These authors contributed equally. (match statement to author names with a symbol)

ACKNOWLEDGMENT

We thank Laure Michelin, Ludovic Josien and Loic Vidal for their assistance with XRD measurements, SEM and TEM observations.

SUPPORTING INFORMATION PARAGRAPH

The additional author names (after the ten) of reference 11 are listed in the supporting information document. This information can be found on the internet at http://pubs.acs.org.

REFERENCES

(1) Elichegaray, C.; Bouallala, S.; Maitre, A.; Ba, M. État et Évolution de la Pollution Atmosphérique. *Revue des Maladies Respiratoires,* **2009**, *26*, 239.

(2) Foster, K.L.; Fuerman, R.G.; Economy, J.; Larson, S.M.; Rood, M.J. Adsorption Characteristics of Trace Volatile Organic Compounds in Gas Streams onto Activated Carbon Fibers, *Chem. Mat.* **1992**, *4*, 1068-1073.

(3) Corma, A. From Microporous to Mesoporous Molecular Sieve Materials and their Use in Catalysis, *Chem. Rev.* **1997**, *97*, 2373-2419.

(4) Corma, A. State of the Art and Future Challenges of Zeolites as Catalysts, *J. Catal.* **2003**, *216*, 298-312.

(5) Choi, M.; Cho, H. S.; Srivastava, R.; Venkatesan, C.; Choi, D.-H.; Ryoo, R. Amphiphilic Organosilane-Directed Synthesis of Crystalline Zeolite with Tunable Mesoporosity, *Nat. Mater.* **2006**, *5*, 718-723.

(6) Srivastava, R.; Choi, M.; Ryoo, R. Mesoporous Materials with Zeolite Framework: Remarkable Effect of the Hierarchical Structure for Retardation of Catalyst Deactivation, *Chem. Commun.* **2006**, 4489-4491.

(7) Choi, M.; Na, K.; Kim, J.; Sakamoto, Y.; Terasaki, O.; Ryoo, R. Stable Single-Unit-Cell Nanosheets of Zeolite MFI as Active and Long Lived Catalysts, *Nature.* **2009**, *461*, 246-249.

(8) Kim, J.; Choi, M.; Ryoo, R. Effect of Mesoporosity Against the Deactivation of MFI Zeolite Catalyst During the Methanol-to-Hydrocarbon Conversion Process, *J. Catal.* **2010,** *269*, 219-228.

(9) Kim, J., Park, W.; Ryoo, R. Surfactant-Directed Zeolite Nanosheets: A High-Performance Catalyst for Gas-Phase Beckmann Rearrangement, *ACS Catal.* **2011**, *1*, 337.

(10) Kabalan, I.; Khay, I.; Nouali, H.; Ryzhikov, A.; Lebeau, B.; Albrecht, S.; Rigolet, S.; Fadlallah, M.-B.; Toufaily, J.; Hamiyeh, T.; et al.Influence of the Particle Sizes on the Energetic Performances of MFI-type Zeolites, *J. Phys. Chem. C.* **2015**, *119*, 18074–18083.

(11) Coasne, B.; Haines, J.; Levelut, C.; Cambon, O.; Santoro, M.; Gorelli, F.; Garbarino, G. Enhanced Mechanical Strength of Zeolites by Adsorption of Guest Molecules, Phys. *Chem. Chem. Phys.* **2011,** *13*, 20096-20099.

(12) Hua, Z.L.; Zhou, J.; Shi, J. L. Recent Advances in Hierarchically Structured Zeolites: Synthesis and Material Performances, *Chem. Commun.* **2011**, *47*, 10536-10547.

(13) Na, K.; Choi, M.; Ryoo, R. Recent Advances in the Synthesis of Hierarchically Nanoporous Zeolites, *Micro. Meso. Mater.* **2013**, *166*, 3-19.

(14) Janssen, A. H.; Koster, A. J.; de Jong, K. P. Three-Dimensional Transmission Electron Microscopic Observations of Mesopores in Dealuminated Zeolite Y, *Angew. Chem. Int. Ed.* **2001,** *40*, 1102-1104.

(15) Dutartre, R.; de Menorval, L. C.; Renzo, F. D.; McQueen, D.; Fajula, F.; Schulz, P. Mesopore Formation During Steam Dealumination of Zeolites: Influence of Initial Aluminum Content and Crystal Size, *Micro. Meso. Mater.* **1996,** *6,* 311-320.

(16) Nesterenko, N. S.; Thibault-Starzyk, F.; Montouillout, V.; Yuschenko, V. V.; Fernandez, C.; Gilson, J. -P.; Fajula, F.; Ivanova, I. I. Accessibility of the Acid Sites in Dealuminated Small-Port Mordenites Studied by FTIR of Coadsorbed Alkylpyridines and CO, *Micro.Meso.Mater.* **2004,** *71*, 157-164.

(17) Groen, J. C. J.; Bach, T.; Ziese, U.; Donk, A. M. P.; de Jong, K. P.; Moulijn, J. A.; Perez-Ramirez, J.Creation of Hollow Zeolite Architectures by Controlled Desilication of Al- Zoned ZSM-5 Crystals, *J. Am. Chem. Soc.* **2005,** *127*, 10792-10793.

(18) Bekyarova, E.; Kaneko, K. Structure and Physical Properties of Tailor-Made Ce,Zr-Doped Carbon Aerogels, *Adv. Mater.* **2000**, *12*, 1625-1628.

(19) Ryoo, R.; Joo, S. H.; Kruk, M.; Jaroniec, M.Ordered Mesoporous Carbons, *Adv. Mater.* **2001**, *13*, 677-681.

(20) Fang, Y.; Hu, H. An Ordered Mesoporous Aluminosilicate with Completely Crystalline Zeolite Wall Structure, *J. Am. Chem. Soc.* **2006**, *128*, 10636-10637.

(21) Fan, W.; Snyder, M. A.; Kumar, S.; Lee, P. -S.; Yoo, W.C.; McCormick, A. V.; Penn, R. L.; Stein, A.; Tsapatsis, M. Hierarchical Nanofabrication of Microporous Crystals with Ordered Mesoporosity, *Nature Mater.* **2008,** *7,* 984-991.

(22) Ciesla, U.; Schuth, F.Ordered Mesoporous Materials, *Micro. Meso. Mater.* **1999**, *27*, 131-149.

(23) Monnier, A.; Schuth, F.; Huo, Q.; Kumar, D.; Margolese, D.; Maxwell, R. S.; Stucky, G. D.; Krishnamurty, M.; Petroff, P.; Firouzi, A.; Janicke, M.; Chmelka, B. F. Cooperative Formation of Inorganic-Organic Interfaces in the Synthesis of Silicate Mesostructures, *Science.* **1993**, *261*, 1299-1303.

(24) Hartmann, M. Ordered Mesoporous Materials for Bioadsorption and Biocatalysis, *Chem. Mater.* **2005,** *17*, 4577-4593.

(25) Xia, Y. D.; Mokaya, R.On the Synthesis and Characterization of ZSM-5/MCM-48 Aluminosilicate Composite Materials*, J. Mater. Chem.* **2004,** *14,* 3427-3435.
(26) Prokesova, P.; Mintova, S.; Cejka, J.; Bein, T.Preparation of Nanosized Micro/Mesoporous Composites via Simultaneous Synthesis of Beta/MCM-48 Phases, *Micro. Meso. Mater.* **2003,** *64*, 165-174.
(27) Galarneau, A.; Cambon, H.; Di Renzo, F.; Ryoo, R.; Choi, M.; Fajula, F. Microporosity and Connections Between Pores in SBA-15 Mesostructured Silicas as a Function of the Temperature of Synthesis, *New J. Chem.* **2003,** *27,* 73- 79.
(28) Na, K.; Choi, M.; Park, W.; Sakamoto, Y.; Terasaki, O.; Ryoo, R. Pillared MFI Zeolite Nanosheets of a Single-Unit- Cell Thickness*, J. Am. Chem. Soc.* **2010,** *132,* 4169-4177.
(29) Na, K.; Jo, C.; Kim, J.; Cho, K.; Jung, J.; Seo, Y.; Messinger, R. J.; Chmelka, B. F.; Ryoo, R. Directing Zeolite Structures into Hierarchically Nanoporous Architectures, *Science.* **2011**, *333,* 328-332.
(30) Machoke, A.G.; Knoke, I.Y.; Lopez-Orozco, S.; Schmiele, M.; Selvam, T.; Marthala, V.R.R.; Spiecker, E.; Unruh, T.; Hartmann, M.; Schwieger, W.Synthesis of Multilamellar MFI-type Zeolites under Static Conditions: The Role of Gel Composition on their Properties*, Micro. Meso. Mater.* **2014,** *190,* 324-333.
(31) Na, K.; Park, W.; Seo, Y.; Ryoo, R.Disordered Assembly of MFI Zeolite Nanosheets with a Large Volume of Intersheet Mesopores, *Chem. Mater.* **2011**, *23*, 1273-1279.
(32) Park, W.; Yu, D.; Na, K.; Jelfs, E.K.; Slater, B.; Sakamoto, Y.; Ryoo, R. Hierarchically Structure-Directing Effect of Multi-Ammonium Surfactants for the Generation of MFI Zeolite Nanosheets, *Chem. Mater.* **2011,** *23*, 5131-5137.
(33) Jung, J.; Jo, C.; Cho, K.; Ryoo, R. Zeolite Nanosheet of a Single-Pore Thickness Generated by a Zeolite-Structure-Directing Surfactant, *J. Mater. Chem.* **2011**, *22*, 4637-4640.
(34) Kabalan, I.; Rioland, G.; Nouali, H.; Lebeau, B.; Rigolet, S.; Fadlallah, M. B.; Toufaily, J.; Hamiyeh, T.; Daou, T. J. Synthesis of Purely Silica MFI-Type Nanosheets for Molecular Decontamination*, RSC Adv.* **2014,** *4,* 37353-37358.
(35) Rioland, G.; Albrecht, S.; Josien, L.; Vidal, L.; Daou, T.J. Influence of the Organosilane Nature and Concentration on the Formation of Hierarchical FAU-Type Zeolite Nanosheets, *New J. Chem.* **2015,** *39,* 2675-2681.
(36) Boltz, M.; Losch, P.; Louis, B.; Rioland, G.; Tzanis, L.; Daou, T.J. MFI-type Zeolite Nanosheets for Gas-Phase Aromatics Chlorination: a Strategy to Overcome Mass Transfer Limitations, *RCS Adv.* **2014,** *4,* 27242-27249.
(37) Schick, J.; Daou, T.J.; Caullet, P.; Paillaud, J.-L.; Patarin, J.; Mangold-Callarec, C.Surfactant-Modified MFI Nanosheets: a High Capacity Anion-Exchanger, *Chem. Commun.* **2011,** *47,* 902-904.
(38) Wu, P.; Debebe, A.; Ma, Y.H. Adsorption and Diffusion of C_6 and C_8 Hydrocarbons in Silicalite, *Zeolites.* **1983,** *3,* 118.
(39) Jacobs, P.; Beyer, H.; Valyon, J. Properties of the End Members in the Pentasil-Family of Zeolites: Characterization as Adsorbents, *Zeolites.* **1981,** *1,* 161-168.
(40) Floquet, N.; Simon, J.M.; Coulomb, J.P.; Bellat, J.P.; Weber, G.; Andre, G.Heptane Adsorption in Silicalite-1: Molecular Dynamics Simulation, *Micro. Meso. Mater.* **2009,** *122,* 61-71.
(41) Lauridant, N.; Daou, T. J.; Arnold, G.; Soulard, M.; Nouali, H.; Patarin, J.; Faye, D.MFI/*BEA Hybrid Coating on Aluminum Alloys, *Micro. Meso. Mater.* **2012,** *152,* 1-8.
(42) Lauridant, N.; Daou, T. J.; Arnold, G.; Nouali, H.; Patarin, J.; Faye, D.Zeolite Hybrid Films for Space Decontamination, *Micro. Meso. Mater.* **2013,** *172,* 36– 43.
(43) Daou, T. J.; Lauridant, N.; Arnold, G.; Nouali, H.; Patarin, J.; Faye, D. Synthesis of MFI/EMT Zeolite Bi-Layer Films for Molecular Decontamination, *Chem. Eng. J.* **2013,** *234,* 66–73.
(44) Cosseron, A. -F.; Daou, T. J.; Tzanis, L.; Nouali, H.; Deroche, I.; Coasne, B.; Tschamber, V. Adsorption of Volatile Organic Compounds in Pure Silica CHA, *BEA, MFI and STT-Type Zeolites, *Micro. Meso. Mater.* **2013**, *173,* 147-154.
(45) Denayer, J.F.; Baron, G.V.; Martens, J.A.; Jacobs, P.A. Chromatographic Study of Adsorption of n-Alkanes on Zeolites at High Temperatures, *J. Phys. Chem. B.* **1998,** *102*, 3077-3081.
(46) Reddy, K.S.N.; Eapen, M.J.; Soni, H.S.; Shiralkar, V.P. Sorption Properties of Cation-Exchanged Beta Zeolites, *J. Phys. Chem.* **1992,***96*, 7923-7928.
(47) Lami, E.B.; Fajula, F.; Anglerot, D.; Des Courieres, T. Single Step Dealumination of Zeolite Beta Precursors for the Preparation of Hydrophobic Adsorbents, *Micro. Mater.* **1993,** *1,* 237-245.
(48) Stelzer, J.; Paulus, M.; Hunger, M.; Weitkamp, J. Hydrophobic Properties of all-Silica Zeolite Beta, *Micro. Meso. Mat.* **1998**, *22,* 1-8.
(49) Dhainaut, J.; Daou, T. J.; Bidal, Y.; Bats, N.; Harbuzaru, B.; Lapisardi, G.; Chaumeil, H.; Defoin, A.; Rouleau, L.; Patarin, J. One Pot Structural Conversion of Magadiite into MFI Zeolite Nanosheets using Mononitrogen Surfactants as Struture and Shape-Directing Agents, *Cryst. Eng. Comm.* **2013,** *15,* 3009-3015.
(50) Camblor, M. A.; Corma, A.; Valencia, S. Synthesis in Fluoride Media and Characterisation of Aluminosilicate Zeolite Beta, *J. Mater. Chem.* **1998**, *8,* 2137-2145.
(51) Lauridant, N.; Daou, T.J.; Arnold, G.; Patarin, J.; Faye, D. MFI/*BEA Hybrid Coating on Aluminum Alloys, *Micro. Meso. Mater.* **2013,** *166*, 79-85.
(52) Rouquerol, F.; Rouquerol, J.; Sing, K. Adsorption by Powders & Porous Solids, Academic Press **1999**.
(53) Thommes, M.; Kaneko, K.; Neimark, A. V.; Olivier, J. P.; Rodriguez-Reinoso, F.; Rouquerol, J.; Sing, K. S. W. IUPAC Technical Report, *Pure Appl. Chem.* **2015**, *87* (9-10), 1051-1069.
(54) Mc Bain, J. W.; Bakr, A. M. A New Sorption Balance, *J. Am. Chem. Soc.* **1926,** *48*, 690–695.
(55) Long, Y.; Jiang, H.; Zeng, H. Sorbate/Framework and Sorbate/Sorbate Interaction of Organics on Siliceous MFI Type Zeolite*, Langmuir.* **1997,** *13,* 4094–4101.
(56) Kirsch-Rodeschini, H. Contrôle de la Contamination Moléculaire par Adsorption sur des Solides Poreux, Ph.D. of the University of Haute Alsace, **2005**.
(57) Xu, D.; Swindlehurst, G. R.; Wu, H.; Olson, D. H.; Zhang, X.; Tsapatsis, M. On the Synthesis and Adsorption Properties of Single-Unit-Cell Hierarchical Zeolites Made by Rotational Intergrowths, *Adv. Func. Mater.* **2014,** *24,* 201 –208.
(58) Ferreira, A. F. P.; Mittelmeijer-Hazeleger, M. C.; Bergh, J. v. d.; Aguado, S.; Jansen, J. C.; Rothenberg, G.; Rodrigues, A. E.; Kapteijn, F. Adsorption of Hexane Isomers on MFI Type Zeolites at Ambient Temperature: Understanding the Aluminium Content Effect, *Micro. Meso. Mat.* **2013,** *170,* 26–35.

(59) Bárcia, P. S.; Silva, J. A. C.; Rodrigues, A. E. Separation of Branched Hexane Isomers Using Zeolite BEA for the Octane Improvement of Gasoline Pool, From Zeolites to Porous MOF Materials – *the 40th Anniversary of International Zeolite Conference*. **2007,** 955-960.
(60) Van Bavel, E.; Meynem, V.; Cool, P.; Lebeau, K.; Vansant, E. F. Adsorption of Hydrocarbons on Mesoporous SBA-15 and PHTS Materials, *Langmuir* **2005**, *21*, 2447-2453.
(61) Zhao, X. S.; Ma, Q.; (Max) Lu, G. Q. VOC Removal: Comparison of MCM-41 with Hydrophobic Zeolites and Activated Carbon, *Energy & Fuels* **1998**, *12*, 1051-1054.
(62) Kärger, J.; Ruthven, D.M. Diffusion in Zeolites and Other Microporous Solids*;* J. Wiley & sons, Inc. New York, 1992.
(63) Groen, J. C.; Zhu, W.; Brouwer, S.; Huynink, S. J.; Kapteijn, F.; Moulijn, J. A.; Pérez-Ramirez, J. Direct Demonstration of Enhanced Diffusion in Mesoporous ZSM-5 Zeolite Obtained Via Controlled Desilication, *J. Am. Chem. Soc.* **2007,** *129,* 355-360.
(64) Gueudré, L.; Bats, N.; Jolimaître, E. Effect of the Surface Resistance on Cyclohexane Uptake Curves in Silicalite-1 Crystals, *Micro. Meso. Mater.* **2012,** *147*, 310-317.